Measurement of the Equation of State of Superfluid Helium-4 at Negative Pressure

Lionel Djadaojee, Cédric Parisi, Camille Noûs, Jules Grucker

Measurement of the equation of state of superfluid helium-4 at negative pressure

Lionel Djadaojee[1], Cédric Parisi[1], Camille Noûs[2], and Jules Grucker*[1]

[1] *Laboratoire Kastler Brossel, ENS-PSL Université, Sorbonne Université, CNRS, Collège de France; 24 rue Lhomond, F-75005 Paris, France.*
[2] *Laboratoire Cogitamus, Paris, France*

Abstract

We report a measurement of the equation of state of superfluid ^{4}He ($T \sim 1$ K) at negative pressure. A stimulated Brillouin gain spectrometer, used together with an optical interferometer, allows us to probe simultaneously both the compressibility and the density of acoustically driven metastable states of the liquid. In the pressure range $0 > P > -1$ bar, the measured equation of state is in agreement with available theories.

1 Introduction

Liquid helium at low temperature is the purest possible liquid. When preparing a sample of liquid ^{4}He in an experimental cell, atomic or molecular impurities other than helium are frozen in the filling line of the cell or on the walls of the cell itself. The only remaining impurities in liquid ^{4}He are helium-3 atoms and their density is very low, typically 0.1 ppm. It is then expected that intrinsic helium-4 phase properties can be studied without being modified by the presence of impurities. In particular, liquid ^{4}He is a model system to probe deep condensed matter metastable states and homogeneous nucleation phenomena. Homogeneous nucleation theory is not only important for condensed matter physics but also for cosmology as it could apply to possible phase transitions in the early universe[1]. The stability limits of superfluid ^{4}He with respect to its gaseous phase have been studied quite intensively both experimentally and theoretically, see for instance the review articles[2, 3] and references therein. Deep metastable states of superfluid ^{4}He are experimentally produced using a high amplitude sound wave focused in the bulk liquid[4, 5, 6, 7, 8, 9]. At acoustic focus and during the negative swing of the wave, the liquid is locally stretched by the acoustic wave and one can thus explore its metastable states where the pressure is expected to be negative[1]. Actually, the measurement of the local pressure of the metastable state is a challenging issue. To date, only estimations of the pressure based on different theoretical assumptions have been published[4, 5, 6, 7, 8]. The purpose of this article is to present a direct measurement of negative pressures in acoustically driven metastable states of liquid helium-4 at $T \sim 1$ K. A consequence of this measurement is the experimental validation in a limited pressure domain of the theoretical equations of state proposed for liquid helium at negative pressures.

2 Experimental setup and procedure

The general idea of this experiment aiming at measuring the local pressure of acoustically driven (meta)stable states of superfluid ^{4}He is to perform a simultaneous measurement of the local density ρ and of the adiabatic bulk modulus $\left.\frac{\mathrm{d}P}{\mathrm{d}\rho}\right|_S$, where P is the pressure of the liquid and S its entropy. Integration of the bulk modulus over the density then gives access to the equation of state (EOS) of the liquid, namely the $P(\rho)$ function.

The experimental set-up consists in three main parts which we shall describe hereafter.

*grucker@lkb.ens.fr, corresponding author.

[1] To picture the concept of negative pressure one may think at a real fluid in a container. When the fluid particles push against the walls of the container, the pressure of the fluid is positive, when they pull against it, it is negative.

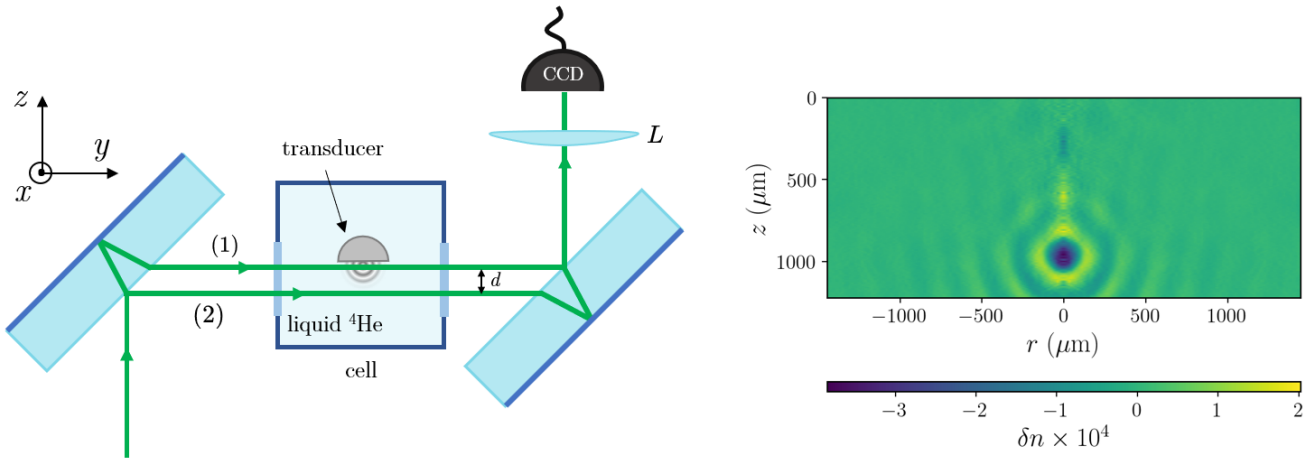

Figure 1: Left: Superfluid ^{4}He metastable state production and density measurement; a convergent acoustic wave is produced in the liquid at $T \sim 1$ K by the excitation of hemispherical transducer. The density modulations near focus are monitored using a Jamin interferometer. The lens L images the acoustic focal region onto the CCD camera. Right: Measurement of the acoustically induced refractive index variation map $\delta_n(r, z)$ at a given ToF t=28.3 μs for a transducer voltage $V = 100$ mV, see text.

2.1 Metastable state production

As mentioned in the introduction of the article, deep metastable states of superfluid ^{4}He are produced using a high amplitude sound wave focused in the bulk liquid[4, 5, 6, 7, 8, 9], see Fig.1 left and Fig.2 left. The experimental cell containing liquid helium is cooled in a cryostat with four optical ports. In the experiment described in this paper, the temperature is fixed at $T = 1.08$ K. Before acoustic excitation, liquid helium is at saturated vapor pressure. A hemispherical piezoelectric transducer excites and focuses ultrasound waves in helium at the resonant frequency $f_{ac} = 1.14$ MHz of its first thickness vibration mode. The transducer inner diameter is 12 mm and the thickness is 2 mm. In order to observe directly the acoustic focus, a small part, 0.9 mm in height, has been removed around the transducer rim. One side of the transducer is grounded and the other side is connected to the output of a RF amplifier driven by an arbitrary function generator (AFG). The excitation voltage of the transducer consists in a train of a harmonic wave voltage at the transducer resonant frequency f_{ac}. The amplitude of the signal delivered by the AFG is noted V.

2.2 Density measurement

Some years ago, our group developed a time resolved quantitative multiphase interferometric imaging technique for measuring the density of a medium inside a sound wave with cylindrical symmetry[10]. This technique has been used to measure the density of metastable states of liquid[8] and solid[11] helium-4 and we shall briefly recall the principle of the measurement now. A Jamin interferometric imaging system is used to measure the density variations imposed to liquid ^{4}He by the focused acoustic wave, see Fig.1. The light source is a pulsed Nd:YAG laser (optical wavelength $\lambda_0 = 532$ nm, temporal width $\tau_0 = 8$ ns, repetition rate $f_0 = 20$ Hz). The acoustic focal region is imaged onto a CCD camera with a magnification factor of 2.5 using an appropriate lens. The spatial resolution[2] of the entire system is 20 μm, about 1/10 of the sound wavelength $\lambda_S \sim 0.21$ mm.

One arm of the interferometer passes through the acoustic focal region while the other crosses the cell in an unperturbed zone.

The acoustic wave introduces a density variation $\delta\rho$ that modulates the refractive index of helium (mainly in the acoustic focus) and hence gives rise to an optical phase shift between the two paths. Using the AFG, we can choose the time t with respect to the sound pulse triggering at which an image of the interference field is taken by the camera. As $\tau_0 \ll 1/f_{ac}$, the images recorded by the CCD camera are to be considered as "snapshots" of the acoustic field. Let y be the light propagation axis, z the transducer symmetry axis, and x the axis orthogonal to y and z (Fig.1). At a given Time of Flight (ToF) t, the acoustically induced phase shift $\delta\phi(x, z)$ map is related to the refractive index map by a simple integration along the y axis. In our case, the sound field is rotationally invariant around the hemisphere

[2]The resolution is defined as the spatial period for which the contrast of a transmission sinusoidal pattern observed through the imaging system is half its maximum.

axis z, so that the refractive index variation δn is only a function of z and $r = \sqrt{x^2 + y^2}$. Given the fact that $\delta n = 0$ outside the sound field, we can write $\delta\phi$ as the Abel transform of δn:

$$\delta\phi(x, z) = \int_{-\infty}^{+\infty} \mathrm{d}y \, \delta n(\sqrt{x^2 + y^2}, z) \tag{1}$$

Conversely, radial refractive index profiles can be retrieved from phase shift maps via an inverse Abel transform[10, 8].

The refractive index n is a function of the density ρ via the Lorentz-Lorenz relation:

$$\frac{n^2 - 1}{n^2 + 2} = \frac{4\pi}{3} \frac{\alpha}{M} \rho \tag{2}$$

where M is the molar weight of ^{4}He (4.0026 g/mol[12]) and α (0.1233 cm^3/mol[13]) is the molar polarizability liquid helium-4 at ~ 1 K [14]. In the limit $n \sim 1$, which is a very good approximation for liquid helium, this relation can be written:

$$\frac{\delta\rho}{\rho_0} = \frac{\delta n}{n_0 - 1} \tag{3}$$

where ρ_0 and n_0 are the density and the refractive index and the unperturbed liquid (no acoustic wave). From the measured quantity δn, the density itself is then easily deduced by $\rho = \rho_0 \left(1 + \frac{\delta n}{n_0 - 1}\right)$. Fig.1 right shows the refractive index variation map measured by this technique at a given time of flight ToF = 28.3 μs for a driving voltage $V = 100$ mV. The corresponding time evolution of the density at a pixel close to the acoustic focus is shown on Fig.4. Note that the technique is based on the reproducibility of the acoustic disturbance as a function of the exciting voltage V. No less than 2000 acoustic pulses are needed to acquire the data of Fig.4[10]. The overall time to register this kind of data is about 10 minutes.

2.3 Brillouin frequency measurement

Metastable states of superfluid ^{4}He are produced on a time scale of less than ~ 400 ns (half period of the sound wave, see Fig.4) and on a spatial scale of less than ~ 100 μm (acoustic focus radius, see Fig.1 right). In order to measure the compressibility of the metastable states of superfluid ^{4}He, we have recently developed a Stimulated Brillouin (SB) gain spectrometer capable of measuring the Brillouin frequencies on such a narrow spatio-temporal domain[15, 16, 17]. Brillouin scattering refers to the scattering of light by a transparent medium due to the coupling of incoming photons with phonons of the material[18]. The energy-momentum conservation in the photon/phonon collision imposes that the Brillouin scattered light is frequency shifted by the amount:

$$f_B = 2n \frac{v}{\lambda} \sin(\theta/2) \tag{4}$$

where n is the refractive index, v is the (adiabatic) speed of sound in the material, λ is the (vacuum) wavelength of the incoming light and θ is the angle between the incoming and the scattered light. f_B is called the Brillouin frequency. Looking at eq.(4), one sees that provided that n, λ and θ are known, measuring f_B provide a way to determine the speed of sound v. SB gain spectroscopy is a pump/probe laser spectroscopy technique to measure f_B. When the frequency difference $f = f_1 - f_2$ between the crossing probe (f_2) and pump (f_1) laser beams is approaching $\pm f_B$, the interfering lasers can create, by electrostriction, phonons at frequency f_B. Light scattering on these phonons results in an energy transfer from the high frequency laser to the low frequency one. Monitoring the probe intensity I_2 as a function of f gives a resonance curve (the Brillouin gain spectrum $g(f)$) of central frequency $\pm f_B$ and width Γ.

The pump laser of our SB spectrometer of central wavelength $\lambda = 1064$ nm is pulsed with a frequency repetition rate of 10 Hz and a pulse duration $\tau = 190$ ns (Full Width at Half Maximum). τ gives the time scale on which Brillouin frequencies are measured. The probe laser is a single frequency CW laser diode also centered at λ tunable over couple of GHz by modulating its feeding current. The spectral resolution of the measurement is about 3.5 MHz given by the linewidth of the beat note between pump and probe fields. The waists of the lasers are about $w_1 \sim w_2 \sim 20$ μm[16]. To minimize the interaction volume, they are crossed at an angle $\theta \sim 90°$ and then superimposed on the acoustic focus, see Fig.2a)[19]. Brillouin frequencies are measured on a space scale of $(2w)^3 = 40^3$ μm^3. We used this SB gain spectrometer to measure the equation of state (EOS) of stable liquid helium-4 between 0 and 10 bar at $T \sim 1$ K by measuring the Brillouin frequency dependence on the static pressure[17]. The experimental EOS obtained is in very good agreement with the theoretical one at $T = 0$ K[20, 21, 22].

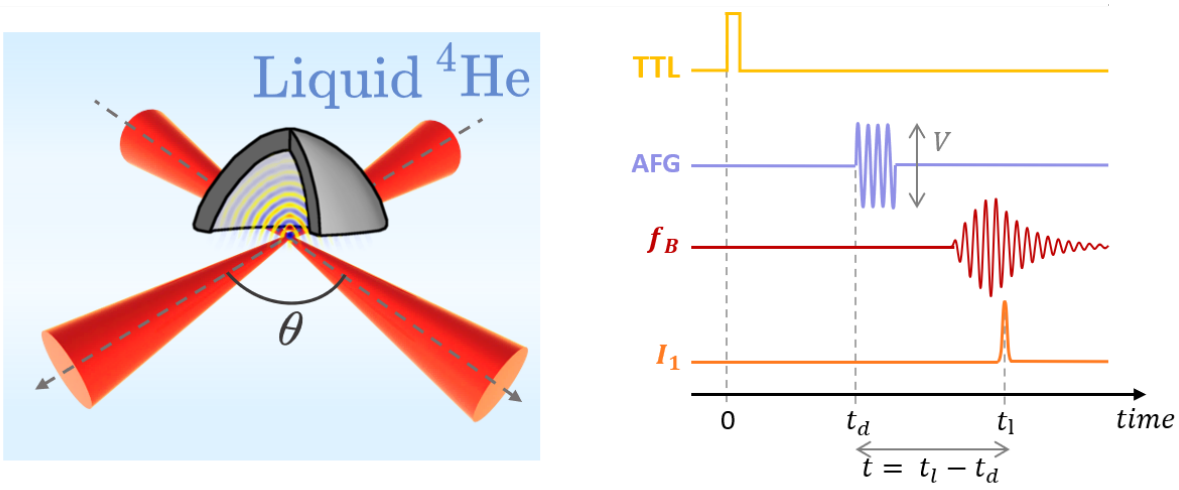

Figure 2: Left: Brillouin frequency measurement: a stimulated Brillouin (SB) gain spectrometer consisting of two crossed laser beams, a pulsed pump and a frequency tuneable CW probe, is used to measure time-resolved Brillouin frequencies of the liquid at acoustic focus. θ is the crossing angle between the lasers. Right: Timeline of the Brillouin measurement: Yellow: 10 Hz clock signal delivered by the SB pulsed pump laser, Purple: driving piezo transducer voltage (amplitude V, frequency f_{ac}), Red: Brillouin frequency at acoustic focus, Orange: Pump SB laser intensity I_1.

The measurement of the Brillouin frequencies in the metastable states of superfluid ^{4}He is though more challenging. We have newly succeeded in doing so by synchronizing the Brillouin frequency measurement with the acoustic wave excitation[19].

The timeline of the Brillouin frequency measurement is sketched on Fig.2 right. The AFG acoustic wave excitation voltage is triggered by a logical clock signal originating from the pulsed pump SB laser (10 Hz repetition frequency). The delay t_d between the trigger pulse and the beginning of the AFG excitation signal can be varied.

The pump laser fires its light pulse of duration τ at a time $t_l \sim 994$ μs after the trigger pulse with a jitter of about $\Delta t_l \sim 0.5$ μs. The actual value of t_l in a given cycle is determined by recording and fitting the temporal intensity profile I_1 of the pump pulse. During the time interval τ, the pump and the probe lasers are interacting with the liquid and the temporal intensity profile of the probe laser I_2 is also recorded. The acoustic wave ToF between the inner part of the transducer and the acoustic focus is given by $t = t_l - t_d$ so that by varying t_d, we build 2-D arrays of data $(t,I_2(t))$. We sample these data in time by interval of $\delta t = 100$ ns. One then gets the Brillouin gain spectrum $g(f,t)$ from which we can extract the corresponding value of the Brillouin frequency $f_B(t)$ as detailed in refs[16, 17]. Finally by varying t we are able to record the time evolution of the Brillouin frequency as the wave propagates through the acoustic focus. Such a time evolution is shown on Fig.4 for an AFG driving voltage $V = 100$ mV. There again note that the technique is based on the reproducibility of the acoustic disturbance as a function of the exciting voltage V as thousands of sound pulses and about 40 minutes are needed to obtain the Brillouin data of Fig.4.

2.4 Quasi simultaneous density and Brillouin frequency measurement

The novelty of the experiment described in this paper is to perform a (quasi) simultaneous measurement of both the density and the Brillouin frequency of the metastable states. These give access to the measurement of the EOS of liquid ^{4}He at negative pressures as we will show after.

A scheme of the optical bench enabling us to perform this simultaneous measurement is shown on Fig.3. As one can see, the Brillouin pump laser (1) is propagating through the cell in the x direction whereas both the Brillouin probe laser (2) and the density measurement green laser (4) are propagating through the cell along the y direction. The key element of this set up is the harmonic beamsplitter (8) which transmits light at wavelength λ_0 (532 nm) and reflects light at wavelength λ (1064 nm). It makes it possible to separate the Brillouin and density signals. For a given excitation AFG voltage V, the time evolution of the Brillouin frequency at acoustic focus is recorded as explained before. Right after the Brillouin measurement, the density measurement is performed for the exact same excitation AFG voltage V. The fact that Brillouin and the density measurements are consecutive in time is the reason why we have described these measurements as being “quasi” simultaneous. But as we have already pointed out, the acoustic

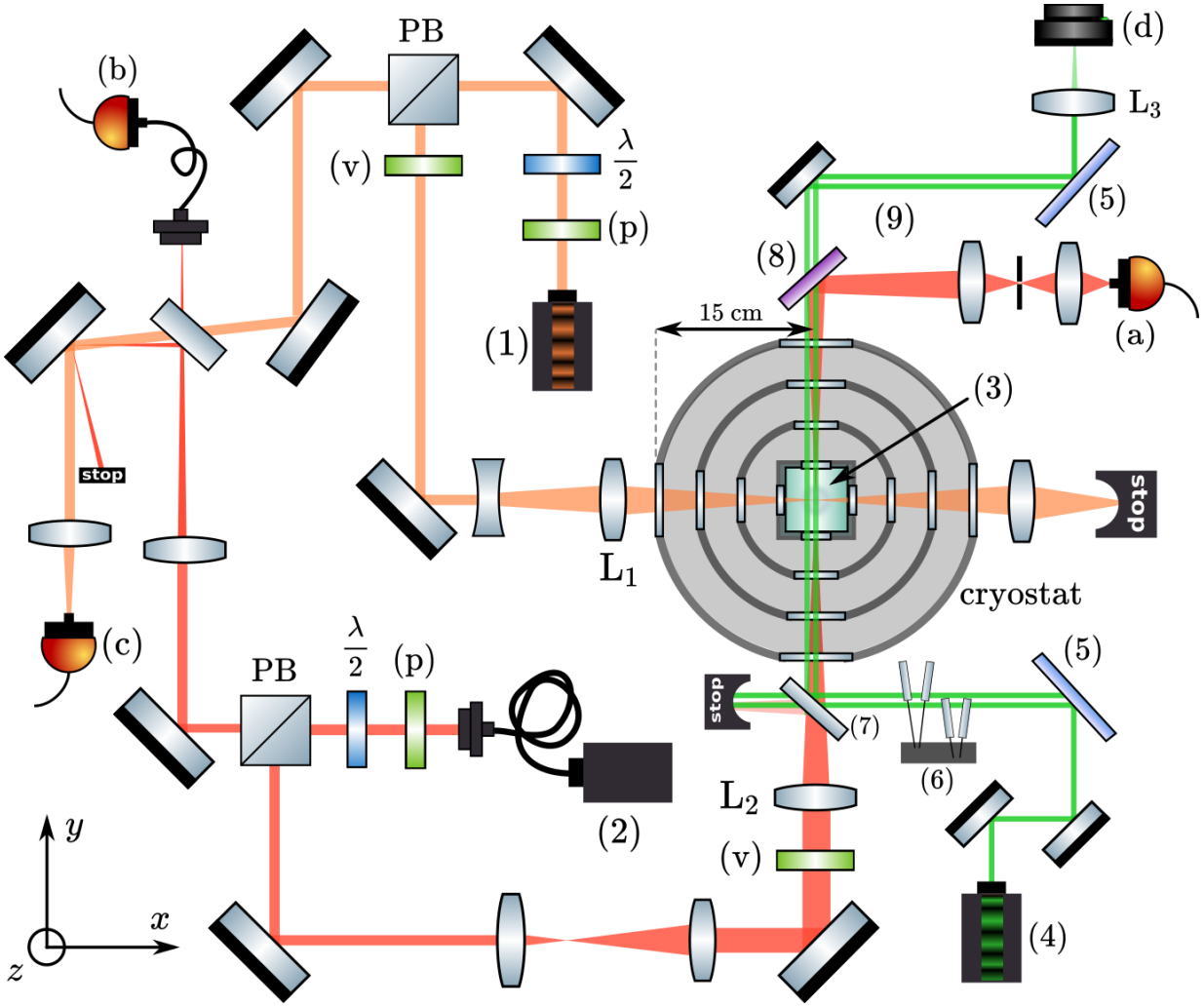

Figure 3: Schematic of the experimental setup. (1): Brillouin Pump laser (infrared pulsed Nd:YAG); (2): Probe laser (infrared CW frequency tunable diode); (3): Sample (superfluid helium-4); (4): Jamin density laser (green pulsed Nd:YAG); (5): Jamin beamsplitter; (6) phase plates; (7) 90/10 Non polarizing beamsplitter; (8) Harmonic beamsplitter transmits $\lambda = 532$ nm light and reflects $\lambda = 1064$ nm light; (a) Brillouin signal photodiode; (b) Brillouin pump photodiode; (c) Brillouin beating signal photodiode; (d) CCD camera (density measurement); (p) linear polarizer; (v) vertical polarizer; $\lambda/2$: half-wave plate; L_1,L_2: Brillouin laser focusing lenses; L_3: density measurement imaging lens.

disturbance of the fluid is a reproducible function of the exciting voltage V and hence it makes no meaning full difference in making those measurements one after the other or rigorously simultaneously.

3 Experimental results and discussion

Fig.4 shows the time evolution of both the Brillouin frequency and of the local density in the close vicinity of the acoustic focus.

To further proceed the data and establish the correspondence between the value of the Brillouin frequency and that of the density, one must find which pixels of the density map corresponds to the Brillouin frequency measurement.

For that, we have proceeded as follows. First of all, we have set the Brillouin lasers so that the volume they probe lies the close vicinity of the acoustic focus. To do so, we send into the liquid intense enough acoustic pulses to induce cavitation (creation of a gas bubble) at acoustic focus[4, 5, 6, 7, 8, 9]. This bubble nucleates at some time t^*, then expands to reach a maximal radius of hundred of μm and finally collapses in a typical lifetime of about 1 ms[9] (much longer than the total duration of the acoustic wave). The bubble strongly scatters the Brillouin lasers and this scattering signal is used for the alignment of the laser beams on the location of the bubble. More precisely in the case of the CW probe beam, the focusing lens L_2 of Fig.3 is mounted on a 3-axis translation stages. To locate the laser

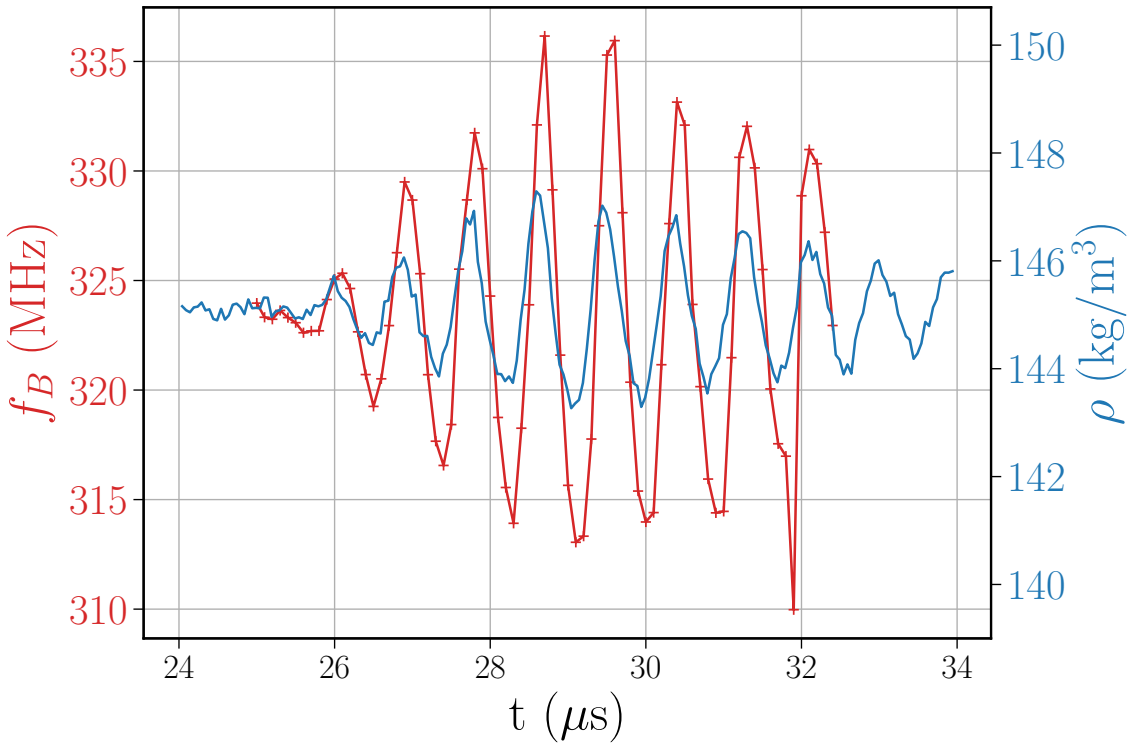

Figure 4: Brillouin frequency and density at acoustic focus versus time for an excitation voltage $V = 100$ mV. Solid red curve: Brillouin frequency. Dotted gray curve: density variations at the pixel where they are of maximal amplitude (see text). Solid blue curve: density variations at a pixel distant 55 μm from the previous one. Note that the phase matching between the red and the blue curve is better than the one between the dotted gray and the red curve.

on the center of the bubble in the (x, z) plane, we act on the (x, z) translations to minimize the starting time of the scattering signal. Indeed, if the laser is off axis with respect to the center of the bubble, the scattering signal will be delayed in regard of t^* as the bubble radius needs a certain time to expand and reach the laser location and scatter it. To align the laser on the center of the bubble in the propagating y direction, one acts on the y translation of the lens L_2 to maximize the amplitude of the scattering signal. The same protocol is applied to the pump laser.

Second, due to the transient nature of the Brillouin excitation[23] during the temporal window of the Brillouin laser pump pulse, a temporal phase shift between the Brillouin signal and the density signal cannot be excluded. The exact magnitude of this phase shift is difficult to compute but its sign can be anticipated. If the Brillouin laser pump pulse was of infinitely short duration, the Brillouin frequency signal would be an instantaneous snapshot measurement of the sound velocity v (see eq. (4) forgetting the negligible contribution of n to the value of f_B) and the Brillouin and the instantaneous density signal would be in phase. But, contrary to the density imaging laser, the Brillouin pump laser has a pulse duration $\tau = 190$ ns which is not negligible with respect to the acoustic period $1/f_{ac} \sim 880$ ns and the sound velocity is thus changing during τ. Let t_0 be a given time of Fig.4 at which the density and the Brillouin frequency are measured. The phonons have a finite lifetime (about hundreds of ns in the stable states[24, 16]). As the stimulated Brillouin signal can only occur when both the pulsed pump laser and the CW probe laser are interacting, the phonons created at the beginning of the pump pulse ($t_0 - \tau/2 \leq t \leq t_0$) will still be present at $t \geq t_0$, and thus contribute more to the measured Brillouin signal than those created at the end of the Brillouin pump pulse ($t_0 \leq t \leq t_0 + \tau/2$). On average, the measured properties of the liquid correspond to a time t_c shorter than t_0. Roughly speaking the measurement of $f_B(t_0)$ is a measurement of $v(t_c)$. Consequently the measured Brillouin signal must be delayed with respect to the (instantaneous) density signal.

Knowing that, we first determine the pixel of the density map whom the density variations are of maximal amplitude. For all pixels whose distance from the maximum density variation pixel is less than 100 μm (typical radius of the acoustic focus), we artificially cancel the temporal phase shift between the Brillouin signal and the density signal by adding a phase φ_a to the latter signal. We then interpolate the $f_B(t)$ measurements on the temporal sampling grid

of the φ_a phase shifted $\rho(t)$ measurement. This allows us to obtain a correspondence between f_B and ρ for each pixel. Because the Brillouin signal is temporally delayed with respect to the density one, we only consider $\varphi_a > 0$ pixels. A map of the phase shift φ_a zoomed on the acoustic focus is shown in the left part of Fig 5.

In order to compare our measurements to available data at positive pressures, we compute the value of the first sound speed from f_B and ρ. This is done thanks to eq.(4) and eq.(2). In the limit $n \sim 1$, we rewrite the Clausius-Mossotti relation (eq.(2)) to read:

$$n(\rho) = \sqrt{1 + \beta\rho} \tag{5}$$

with $\beta = \dfrac{4\pi\alpha}{M} = 3.871(3)\,10^{-4}$ m^3/kg. Inserting eq.(5) in eq.(4) and evaluating it for $\rho = \rho_0$ and $\rho \neq \rho_0$, one gets:

$$v(\rho) = v(\rho_0)\frac{f_B(\rho)}{f_B(\rho_0)}\sqrt{\frac{1+\beta\rho_0}{1+\beta\rho}} \tag{6}$$

where ρ_0, $v(\rho_0)$ and $f_B(\rho_0)$ are respectively the density, the sound velocity and the Brillouin frequency at thermal equilibrium (no acoustic wave, $V = 0$ mV). At $T = 1.08$ K and saturated vapor pressure, $\rho_0 = 145.12(1)$ kg/m^3 and $v(\rho_0) = 237.6(1)$ m/s are well tabulated quantities[25] and we have measured the Brillouin frequency without acoustic wave and found $f_B(\rho_0) = 323.1(4)$ MHz. For all pixels within the radius of the acoustic focus we compute the $v(\rho)$ curves. We have recently measured the Brillouin frequencies of statically pressurized superfluid helium at $T \sim 1$ K[17]. From this work it is possible to extract the actual first sound velocity to density dependence of stable $P > 0$ liquid ^{4}He at $T \sim 1$ K and compare it to the $v(\rho)$ curves we obtain for each pixel. The right part of Fig.5 displays $v(\rho)$ curves in stable thermodynamic states ($\rho > \rho_0$). The red data points correspond the measurements of ref.[17]. The colored lines corresponds to linear fits of the $v(\rho)$ dependency at the corresponding colored pixel of the left part of Fig.5. It is seen that all these $v(\rho)$ fits are compatible with the results of ref.[17]. Hence, to determine the EOS in the stable and metastable domains, we consider the $v(\rho)$ data corresponding to all those pixels. Those data points are plotted in Fig.6. Quadratic or higher order polynomial fits do not give better results than the plotted linear fit.

Having the $v(\rho)$ curve, it is quite straightforward to determine the EOS of acoustically driven stable and metastable states of superfluid ^{4}He at $T \sim 1$ K. For a material of density ρ at a pressure P, the (adiabatic) sound velocity v is linked to the (adiabatic) compressibility of the material through the relation[26]:

$$v^2 = \left.\frac{\partial P}{\partial \rho}\right|_S \tag{7}$$

where S is the entropy of the material. Fig.(6) is a measurement of the sound velocity to density dependence within an acoustic wave, that is at constant entropy of the liquid. A simple integration of eq.(7) gives access to the EOS, that is to the $P(\rho)$ function.

Setting $v(\rho) = a\rho + b$ with $a = 4.67(6)$ m^4/kg/s and $b = -440(9)$ m/s the fit function displayed in Fig.6, we analytically integrate eq.(7) from the known initial thermal equilibrium state (ρ_0,v_0,P_0) to a final state (ρ,v,P) to get:

$$\int_{P_0}^{P} \mathrm{d}P' = \int_{\rho_0}^{\rho} (a\rho' + b)^2\,\mathrm{d}\rho' \tag{8}$$

$$P(\rho) = P_0 + \frac{1}{3a}\left[(a\rho + b)^3 - (a\rho_0 + b)^3\right] \tag{9}$$

This experimental $P(\rho)$ function is plotted on Fig.7. The error bars on the pressure are calculated from the uncertainties on the a and b coefficients of the $v(\rho)$ fit function. They are slightly smaller than the data points. On the figure is also plotted Dalfovo *et al.* density functional theory giving the EOS of positive and negative pressure states of superfluid ^{4}He at $T = 0$ K. Note that other computational methods have been used to compute the EOS in the $T \to 0$ limit [21, 22] which all agree to Dalfovo's within 1 % but don't provide an explicit analytic form of the EOS.

Regarding the positive pressure stable states in Fig.7, the satisfactory theory-experiment agreement arises from the fact that we have used the results of ref.[17] to find the pixels of the density map which corresponds to Brillouin frequency measurement. As the positive pressure EOS determined in ref.[17] was in agreement with Dalfavo's theory, it is no surprise that our measurement is also in agreement with Dalfovo's theory in the stable part of the phase diagram.

Regarding the negative pressure metastable states, one first stresses that we have been able to measure negative pressures of acoustically driven metastable states of liquid ^{4}He. This direct experimental measurement of the EOS of metastable liquid helium-4 allows us to test the relevance of existing theoretical equation of states in the negative

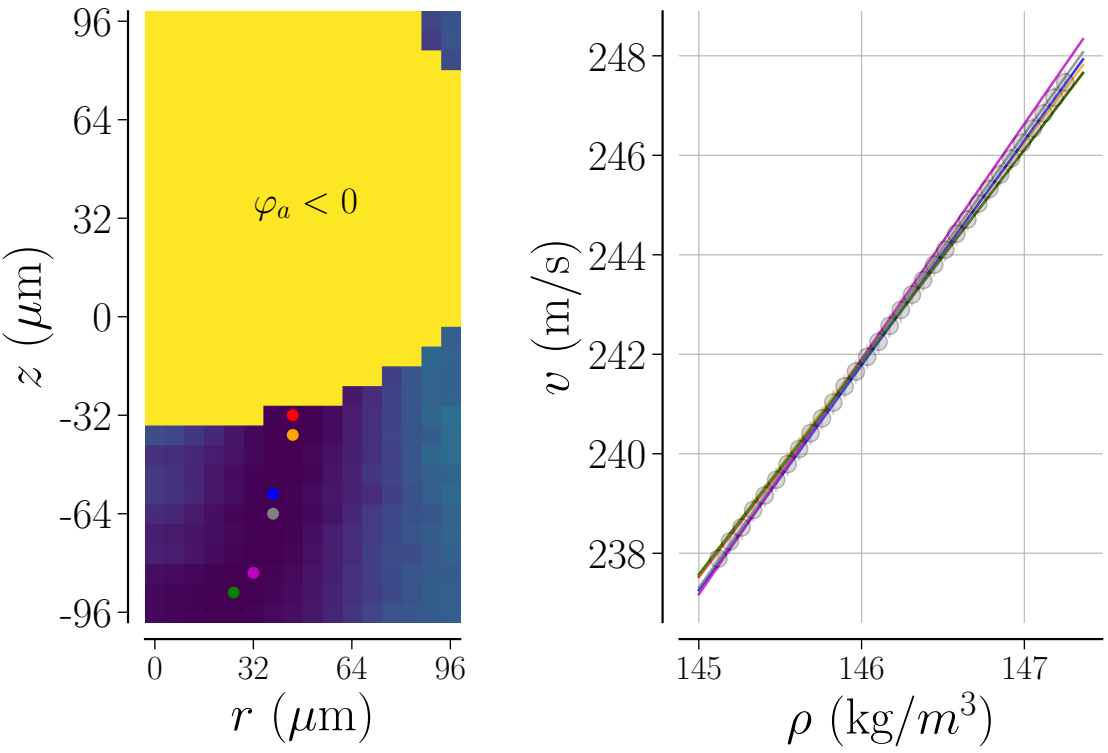

Figure 5: Left: φ_a map at acoustic focus (see text): yellow area : $\varphi_a < 0$, blue area: $\varphi_a > 0$. Right: Sound velocity to density dependence in stable states ($\rho > \rho_0$) of superfluid ^{4}He at $T \sim 1$K; grey data points: measurements of ref.[17], colored lines: linear fits of the $v(\rho)$ dependency measured within the acoustic wave ($\rho > \rho_0$) at the corresponding colored pixel of the left part of the figure.

pressure domain. For pressures $0 > P > -1$ bar, the good agreement between our experimental data and Dalfovo's theory enables us to conclude that available $T = 0$ K theoretical EOSs[20, 21, 22, 27] satisfactorily reproduce the pressure-density dependence of metastable states of liquid ^{4}He at ~ 1 K. Note that temperature changes due to adiabatic compression and decompression phases are not important enough to observe a disagreement between the measured equation of state and the theoretical equation of state at $T = 0$ K. Those temperature changes are theoretically supposed to be less than 30 mK[27].

4 Conclusion

Using an optical interferometer together with a stimulated Brillouin gain spectrometer, we have measured simultaneously both the density and the compressibility of acoustically driven (meta)stable states of liquid ^{4}He at ~ 1 K. This enabled us to experimentally determine the equation of state of the liquid submitted to the acoustic disturbance and allows us to test the relevance of theoretical EOS of metastable states of liquid ^{4}He by comparison of our measurement with theoretical predictions. We found that available theoretical 0 K EOS of liquid ^{4}He at negative pressure correctly reproduce experimental data for the pressure range $0 > P > -1$ bar. This set up will be used to measure the EOS of deep metastable states of liquid ^{4}He at ~ 1 K in the close vicinity of the destabilization (cavitation) threshold where deviations between the actual EOS and the theoretical one are suspected[19].

Acknowledgement

We thank F. Perrin and O. Andrieu for cryogenics support and T. Tardieu, S. Dubois, C. Rio and A. Gohlke for logistic support. This work has been funded by the french Ministère de l'Enseignement Supérieur et de la Recherche.

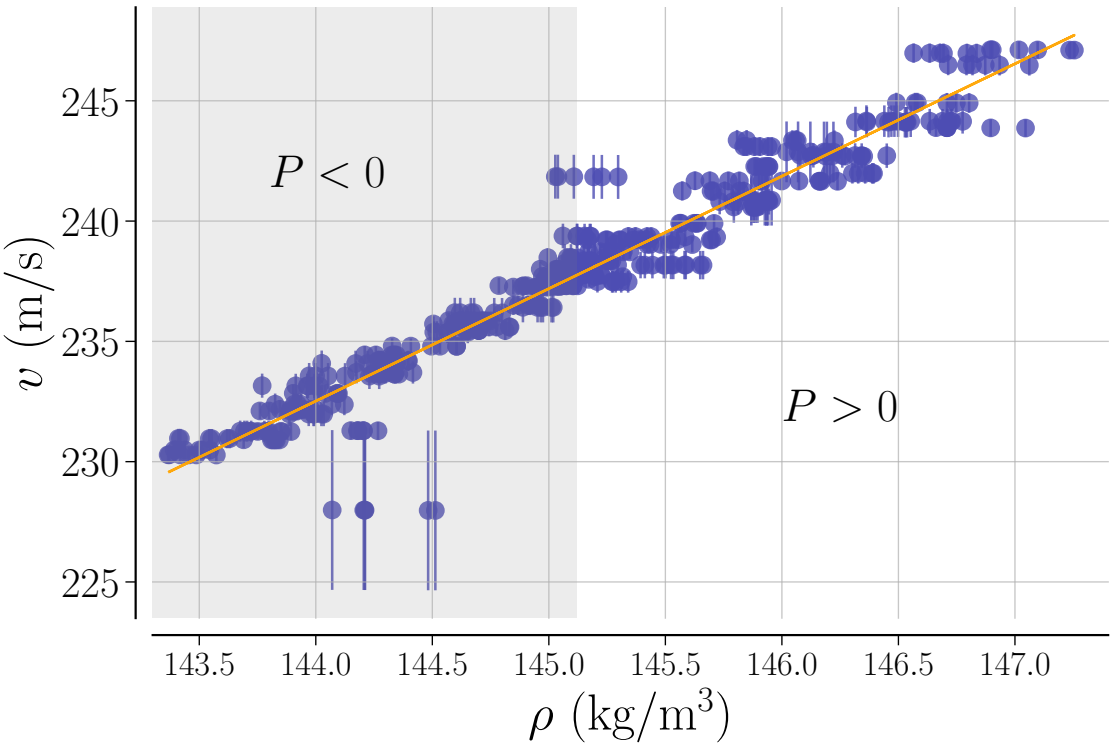

Figure 6: Sound velocity versus density in the vicinity of the acoustic focus. Solid blue circles: experimental data; orange line: linear fit. Shaded area: metastable negative pressure domain; non shaded area: stable positive pressure domain.

References

[1] D. Boyanovsky, H. de Vega, D. Schwarz, Annual Review of Nuclear and Particle Science **56**(1), 441 (2006). DOI 10.1146/annurev.nucl.56.080805.140539

[2] S. Balibar, J. Low Temp. Phys. **129**(5), 363 (2002). DOI 10.1023/A:1021412529571. URL `https://doi.org/10.1023/A:1021412529571`

[3] J. Grucker, J. Low Temp. Phys. **197**(3), 149 (2019). DOI 10.1007/s10909-019-02212-8. URL `https://doi.org/10.1007/s10909-019-02212-8`

[4] J.A. Nissen, E. Bodegom, L.C. Brodie, J.S. Semura, Phys. Rev. B **40**(10), 6617 (1989). DOI 10.1103/PhysRevB.40.6617

[5] Q. Xiong, H.J. Maris, JLTP **82**, 105 (1991). DOI https://link.springer.com/article/10.1007/BF00681524

[6] Lambaré, H., Roche, P., Balibar, S., Maris, H. J., Andreeva, O. A., Guthmann, C., Keshishev, K. O., Rolley, E., Eur. Phys. J. B **2**(3), 381 (1998). DOI 10.1007/s100510050261. URL `https://doi.org/10.1007/s100510050261`

[7] F. Caupin, S. Balibar, Phys. Rev. B **64**, 064507 (2001). DOI 10.1103/PhysRevB.64.064507. URL `http://link.aps.org/doi/10.1103/PhysRevB.64.064507`

[8] A. Qu, A. Trimeche, J. Dupont-Roc, J. Grucker, P. Jacquier, Phys. Rev. B **91**(21), 214115 (2015). DOI https://journals.aps.org/prb/abstract/10.1103/PhysRevB.91.214115

[9] A. Qu, A. Trimeche, P. Jacquier, J. Grucker, Phys. Rev. B **93**(17), 174521 (2016). DOI https://journals.aps.org/prb/abstract/10.1103/PhysRevB.93.174521

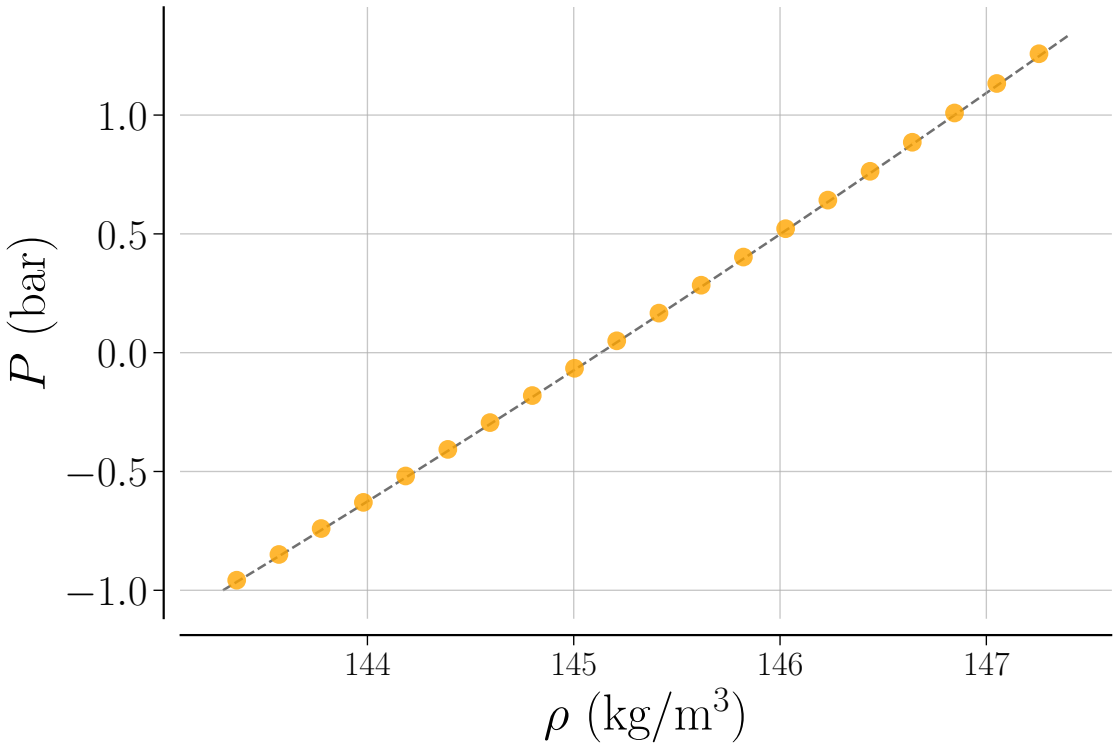

Figure 7: EOS of superfluid ^{4}He at $T \sim 1$ K. Full orange circles: experimental data, error bars are smaller than the symbols; dotted gray line: theory at 0 K[20].

[10] F. Souris, J. Grucker, J. Dupont-Roc, P. Jacquier, A. Arvengas, F. Caupin, Appl. Opt. **49**, 6127 (2010). DOI 10.1364/AO.49.006127

[11] F. Souris, J. Grucker, J. Dupont-Roc, P. Jacquier, Europhys. Lett. **95**(6), 66001 (2011). DOI https://epljournal.edpsciences.org/articles/epl/abs/2011/18/epl13806/epl13806.html

[12] National Center for Biotechnology Information, (2020). URL `https://pubchem.ncbi.nlm.nih.gov/element/Helium`

[13] R.F. Harris-Lowe, K.A. Smee, Phys. Rev. A **2**, 158 (1970). DOI 10.1103/PhysRevA.2.158. URL `https://link.aps.org/doi/10.1103/PhysRevA.2.158`

[14] B.M. Abraham, Y. Eckstein, J.B. Ketterson, M. Kuchnir, P.R. Roach, Phys. Rev. A **1**, 250 (1970). DOI 10.1103/PhysRevA.1.250. URL `https://link.aps.org/doi/10.1103/PhysRevA.1.250`

[15] L. Djadaojee, A. Douillet, J. Grucker, Eur. Phys. J. Appl. Phys. **89**(3), 30701 (2020). DOI 10.1051/epjap/2020200012. URL `https://doi.org/10.1051/epjap/2020200012`

[16] L. Djadaojee, A. Douillet, J. Grucker, J. Low Temp. Phys. **203**(1), 234 (2021). DOI 10.1007/s10909-021-02584-w. URL `https://doi.org/10.1007/s10909-021-02584-w`

[17] L. Djadaojee, J. Grucker, Phys. Rev. B **103**, 144513 (2021). DOI 10.1103/PhysRevB.103.144513. URL `https://link.aps.org/doi/10.1103/PhysRevB.103.144513`

[18] L. Brillouin, Ann. Phys. **9**(17), 88 (1922). DOI 10.1051/anphys/192209170088. URL `https://doi.org/10.1051/anphys/192209170088`

[19] L. Djadaojee, J. Grucker, Phys. Rev. Lett. **129**, 125301 (2022). DOI 10.1103/PhysRevLett.129.125301. URL `https://link.aps.org/doi/10.1103/PhysRevLett.129.125301`

[20] F. Dalfovo, A. Lastri, L. Pricaupenko, S. Stringari, J. Treiner, Phys. Rev. B **52**, 1193 (1995). DOI 10.1103/PhysRevB.52.1193. URL http://link.aps.org/doi/10.1103/PhysRevB.52.1193

[21] J. Boronat, J. Casulleras, J. Navarro, Phys. Rev. B **50**, 3427 (1994). DOI 10.1103/PhysRevB.50.3427. URL http://link.aps.org/doi/10.1103/PhysRevB.50.3427

[22] G.H. Bauer, D.M. Ceperley, N. Goldenfeld, Phys. Rev. B **61**, 9055 (2000). DOI 10.1103/PhysRevB.61.9055. URL http://link.aps.org/doi/10.1103/PhysRevB.61.9055

[23] R.W. Boyd, *Nonlinear Optics*, 3rd edn. (Academic Press, Inc., Orlando, FL, USA, 2008)

[24] P. Berberich, P. Leiderer, S. Hunklinger, Journal of Low Temperature Physics **22**(1), 61 (1976). DOI 10.1007/BF00655215. URL https://doi.org/10.1007/BF00655215

[25] R.J. Donnelly, C.F. Barenghi, J. Phys. Chem. Ref. Data **27**, 1217 (1998). DOI https://doi.org/10.1063/1.556028

[26] L.D. Landau, E.M. Lifshitz, *Statistical Physics, Part 1*, *Course of Theoretical Physics*, vol. 5 (Butterworth-Heinemann, Oxford, 1980)

[27] H.J. Maris, D.O. Edwards, J. Low Temp. Phys. **129**, 1 (2002). DOI https://link.springer.com/article/10.1023/A:1020060700534